

Sea clutter encountered in littoral environments

An analysis of low grazing angle open ocean sea clutter, based on a simple characterisation of the clutter in terms of scattering from ripples riding on long waves (the composite model) and from breaking waves, is extended to clutter encountered in littoral environments. The modelling of the scattering itself is unchanged; modification of the sea surface waves by limited fetch, wave refraction, current variations and enhanced breaking in shallow water affect the scattering structures significantly. Here we characterise the phenomena involved through relatively simple physical models that allow complicated and realistic environments to be modelled.

By

K. D. Ward and R. J. A. Tough

TW Research Ltd, Harcourt Barn, Harcourt Road, Malvern, WR14 4DW

Introduction

The operation of maritime radar systems close to the coast is affected by the characteristics of the radar reflections from the sea surface, known as sea clutter. Experimentally it has been found that the sea clutter in these littoral environments is different from that in the open ocean, and often causes degradation in radar performance. The successful method used to model sea clutter empirically in the open ocean, by taking many measurements and looking for trends in behaviour as a function of viewing direction and sea conditions, is difficult to repeat in the littoral. This is because there are too many factors affecting the behaviour, as each environment is different. To make progress it is necessary to model the behaviour of the sea surface in littoral conditions and then to calculate radar scattering from that surface. The resulting modelled behaviour of sea clutter may then be analysed for measurable trends, which can be verified empirically.

In this paper we investigate such an approach applied to low radar grazing angles, typical of radar systems operating from aircraft or ships. We consider back-scattering from the sea surface but, except for local forward scattering causing interference at the surface, do not include propagation effects that are important for some types of radar. Two sections on the description of the sea surface in the open ocean are followed by an outline of the radar cross section (RCS) modelling technique and results. The four principal processes that change the character of the sea surface in the littoral environment are then described along with how to extend RCS modelling to these conditions. Initial results of the effect of limited fetch on RCS are presented.

Ocean wave spectrum

The hydrodynamic description of the sea surface and its interaction with the wind is a problem of such complexity that its complete solution is not currently possible. To make progress towards a physically useful model, simplifying assumptions must be made. The most common approximation is to linearise the hydrodynamic equations for surface waves and to obtain the solutions of small amplitude, sinusoidal waves. As the system is approximately linear the overall sea structure may be modelled as the superposition of many such waves, resulting in a Gaussian noise process for the wave height. The energy of the waves at each spatial frequency, \mathbf{k} , is characterised in terms of a power spectrum, $S(\mathbf{k})$, where the mean square of the overall wave height, η , resulting from the sum of all the wave components may be derived from the integral over \mathbf{k} ,

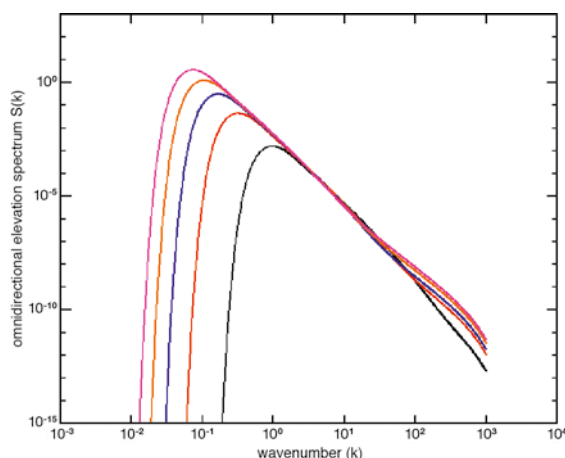
Equation 1

$$\langle \eta^2 \rangle = \int d^2 k S(\mathbf{k}).$$

There are many forms of $S(\mathbf{k})$ that are derived from experimental measurements. The Elfouhaily spectrum [1] is particularly good because it incorporates a wide range of observed characteristics.

Figure 1 shows the omnidirectional form of the spectrum, which is obtained by integrating $S(\mathbf{k})$ over the direction of the wave vector \mathbf{k} . The plot shows five sea states (1 to 5), which correspond to mature seas with wind speeds of 3.2, 5.5, 7.6, 9.6 and 11.5 metres per second. The longest waves in the spectrum (i.e., at the smallest k) correspond to waves travelling at the wind speed. Thus we see that the left-most line (with the longest waves) is sea state 5 and the right-most line is sea state 1. Above the long wave cut-off, the form of the spectrum is approximately the same at all sea states, except for a slight modulation at very short waves (high k). In the middle region the wave spectrum is said to be saturated, with an equilibrium existing between wave generation by the wind and dissipation by wave breaking and viscous damping.

1



The Elfouhaily omnidirectional wave spectrum for sea states 1 to 5.

Summing all of the waves together produces a sea surface modelled as a Gaussian random field. This reproduces some of the visual features of the sea surface, particularly when supplemented by dynamics governed by the correct wave dispersion relation. However a Gaussian distribution of surface height fluctuations is symmetric about its mean, and is unable to capture the essentially asymmetric, choppy character of the sea surface or breaking wave phenomena.

Choppy and breaking waves

In our earlier work [2] we adopted the Gaussian sea surface model described in the previous section. The power spectrum $S(\mathbf{k})$ can be related directly to the mean square value of the vertical acceleration of the sea surface, which again has Gaussian statistics. Setting a threshold on this acceleration of $-g/2$ allowed us to identify the onset breaking wave events on the basis of a physically well-founded criterion and relate the probability of their occurrence directly to prevailing conditions.

A linearised hydrodynamic description [3] of the incompressible and irrotational flow in an ocean of infinite depth identifies a localised circular fluid motion, whose amplitude falls off with depth. In a simple one-dimensional geometry this in turn establishes a trochoidal form for the surface wave profile, as was first described by Gerstner many years ago [4]. More recently Creamer et al [5] investigated non-linear canonical transformations of the equations of motion of the surface height and velocity potential appropriate to the description of an irrotational breaking wave and identified variables that are described by the linearised equations of hydrodynamics to a very good approximation. Inversion of their solution yields results for the actual surface height and velocity potential that capture many of the non-linear features of their dynamics. For one-dimensional, corrugated, waves this inversion coincides with the Gerstner construction, which also provides a useful approximation in the more general, two-dimensional, case. In order to eliminate the more strikingly unrealistic features of our earlier model, and still retain some of its computational tractability, we have adapted the Gaussian random field, subjecting the support \mathbf{x} of each of its harmonic components, with a complex amplitude $\tilde{h}(\mathbf{k})$ specified by the power spectrum, to the transformation

Equation 2

$$\mathbf{x} \rightarrow \mathbf{x} + \frac{i\mu}{(2\pi)^2} \int d^2k \frac{\mathbf{k}}{k} \tilde{h}(\mathbf{k}) \exp(-i\mathbf{k} \cdot \mathbf{x}) = \mathbf{x} + \mu \mathbf{D}(\mathbf{x})$$

$$\langle \tilde{h}(\mathbf{k}) \tilde{h}(\mathbf{k}') \rangle = (2\pi)^4 \delta(\mathbf{k} + \mathbf{k}')$$

This procedure has been suggested by Tessendorf [6], and is widely used in CGI where it produces strikingly realistic effects (see Figure 2). The partial derivatives,

Equation 3

$$J_{xx} = 1 + \mu \frac{\partial D_x(\mathbf{x})}{\partial x}$$

$$J_{yy} = 1 + \mu \frac{\partial D_y(\mathbf{x})}{\partial y},$$

$$J_{xy} = J_{yx} = \mu \frac{\partial D_y(\mathbf{x})}{\partial x}$$

constitute a correlated tri-variate Gaussian. The mean values of J_{xx}, J_{yy}, J_{xy} are 1,1,0 respectively. Their covariance matrix has elements that can be evaluated in terms of the power spectrum of the sea surface height fluctuations e.g.

Equation 4

$$\langle J_{xy}^2 \rangle = \mu^2 \int d^2k \frac{k_x^2 k_y^2}{k^2} S(\mathbf{k})$$

The Jacobian determinant for the transformation (2) can be constructed from (3); Tessendorf suggests that its taking negative values be identified as a criterion for wave breaking, which can be controlled through the parameter μ . In our work we have set μ to unity and identified the value of $1/2$ as a more appropriate threshold. This coincides with the previously used acceleration threshold when the sea surface has a one-dimensional corrugated structure; the Gerstner wave satisfying this threshold criterion also nestles comfortably in the 120° apex of the Stokes corner wave, which has been identified as a precursor to a breaking wave [7].

2



Sea surface simulation by superposition of Gerstner waves.

The calculation of the breaking area in this model is more complicated than that based on the acceleration threshold. Nonetheless the statistics of the Jacobian J can be analysed, most conveniently in terms of the characteristic function

Equation 5

$$C(\omega) = \langle \exp(i\omega J) \rangle;$$

the probability that wave breaking occurs is then given by

Equation 6

$$\frac{1}{2} + \frac{i}{2\pi} \text{PP} \int_{-\infty}^{\infty} \frac{C(\omega)}{\omega} \exp(-i\omega/2) d\omega$$

The details of this analysis are rather involved [8]. Nonetheless its results allow us to evaluate the breaking area quite simply in terms of quantities that relate directly to the power spectrum. In the special case where the power spectrum is isotropic the analysis simplifies significantly; the breaking area now depends on a single parameter that also determines the mean square vertical acceleration, and comparable, though not identical, results are obtained from the two criteria. Tessendorf's negative Jacobian criterion predicts very small breaking areas, if we set μ to one.

EM Scattering and clutter RCS

Research on EM scattering at low grazing angles [2] has shown that the average RCS may be calculated with reasonable accuracy by summing the contribution of two components:

- Resonant scattering from ripples modulated by the long wave slope (the composite model), and
- Diffuse scattering from breaking waves.

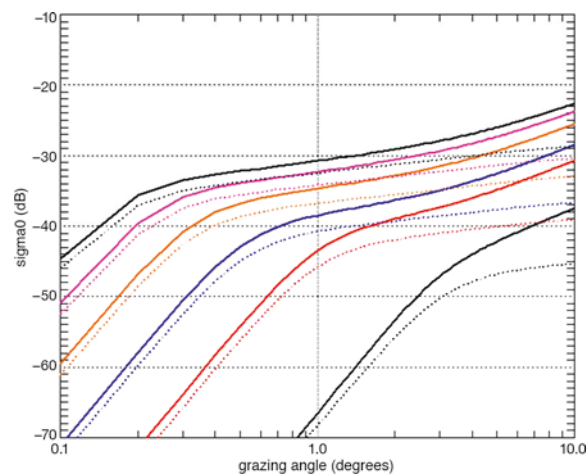
Both of these components are subject to multipath illumination, which is implemented using Katzin's critical angle [9], and a power law attenuation for shadowing. The composite model calculations use the wave power spectrum, as discussed above. The spectrum is split into short and long waves (the division being at approximately the radar wavelength). The short wave produce polarisation and angular dependent backscatter, modelled using small perturbation theory, from waves at about half the radar wavelength. This is then modulated by the distribution of incidence angles caused by the slopes (derived from the long wavelength portion of

the spectrum). The breaking wave calculations are based on numerical calculations of scattering from very rough surfaces and the percentage of the sea area covered by breaking waves; the latter is calculated using the wave spectrum and the breaking wave criterion discussed above. More details of these calculations are given in reference [10].

Figure 3 shows results calculated of the open ocean normalised RCS at X-band (9 GHz) for sea state 1 (lowest NRCS line) to sea state 6 (highest RCS line). The solid lines are VV and the dotted lines HH polarisation. These results match well to the GIT empirical model, derived from well calibrated real sea clutter data.

These scattering results may be extended up to about 70 degrees grazing using the same model, although the breaking waves make little contribution above 15 degrees and can be ignored along with the shadowing and multipath. Hence the composite model alone produces good results. Above 70 degrees the effects of specular scattering begin to become apparent and methods based on physical and geometric optics provide better results.

3



Normalised radar cross section versus grazing angle calculated for sea states 1 to 6 with vertical (solid lines) and horizontal (dotted lines) polarisations.

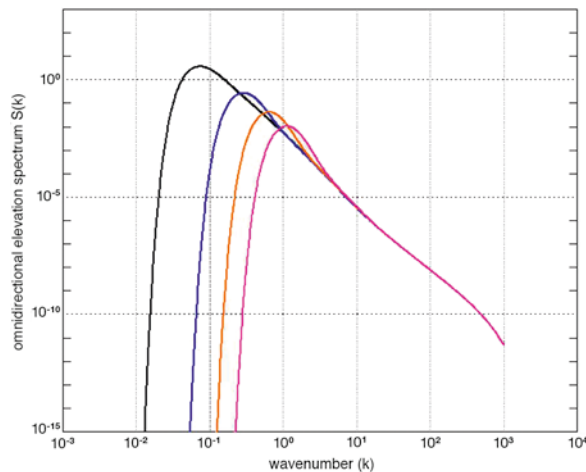
Littoral water effects

Having established the basic tools for modelling the wave spectrum, wave breaking and sea clutter RCS, we now consider changes that occur in littoral environments.

Waves in coastal waters often only have a short distance to interact with the wind. Thus the long waves do not have time to form, and the shorter waves have a more choppy appearance. This phenomenon is characterised as limited fetch and the resulting sea is described as ‘young’ or ‘immature’. The effect on the wave spectrum is as shown in Figure 4. The rightmost line shows a mature sea corresponding to Figure 1. When the fetch is reduced progressively for the other curves, we see that the long waves do not have time to develop and thus the low- k cut off increases in value. This has the effect of reducing the area under the curve and thus decreasing the rms wave height.

Another effect (evident in Figure 4) of reducing the fetch is the longest wave spectral densities being above the saturation curve of the mature sea. This causes increased breaking at these wavelengths and is part of the process whereby the wave energy is transferred to longer waves (lower k); the so-called down-shifting process. When the longest waves are travelling at the wind speed this process stops and the sea is in equilibrium. The wave spectra for limited fetch in Figure 4 are used to derive NRCS trends below in section 6.

4



Omnidirectional wave spectra for a wind speed of 11.5 m/s and fetches of 1.5 km (rightmost line), 4 km, 20 km, and greater than 100 km.

Ocean waves obey a dispersion relation, which expresses the temporal frequency, ω , in terms of the spatial frequency, k . The dispersion relation causes waves at different frequencies to travel at different speeds, through $v = \omega/k$. In deep water the dispersion relation is $\omega^2 = gk$, whilst in water of depth d this changes to

Equation 7

$$\omega^2 = gk \tanh(kd)$$

When a wave train propagates into a region of different depth its frequency remains constant, but the wavelength and amplitude change. (Equation 7 shows that it is only long wavelengths, of greater than about twice the depth, that are affected by this process). At a given temporal frequency we can write the velocity in terms of an effective refractive index, n ,

Equation 8

$$v(d) = \frac{v(\infty)}{n(d)},$$

and solve the problem using Fermat's principle as in geometric optics. The method is described by Gamito and Musgrave [11] and allows the energy of long waves propagating in coastal environments to be calculated.

In littoral environments the coastline and depth variations often result in spatially varying tidal currents. These cause changes to the wave spectrum, typically at wavelengths in the order of a metre. When a wave train propagates into a region of changing current, energy is exchanged between the wave and the current, and the property that is conserved is the ‘wave action’ defined by

Equation 9

$$\phi = \frac{E}{\omega}.$$

This process changes the wave spectrum of the sea and therefore moves it out of equilibrium with the wind. Thus the wind acts to restore the equilibrium and, since the waves affected are of modest wavelength, this happens over a relatively short distance (tens to hundreds of metres). The overall process is termed 'action-balance' and is modelled by integrating a differential equation defining the behaviour of the wave spectral density over rays following the wave energy at the group velocity plus the current. The details of this method are described chapter 3 of reference [10] and other references contained therein. The effects of current variations are often clearly evident on radar imagery from remote sensing satellites to low grazing angle airborne radar [12].

The deep-water analysis that led us to identify the trochoidal Gerstner surface wave can also be modified to take account of finite depths. The circular fluid motion characteristic of deep waters now becomes elliptical; the motion perpendicular to the gravitational restoring force driving the surface waves is enhanced.

A constant frequency ω establishes infinite depth limiting group velocity and wavenumber of

Equation 10

$$c_g(\infty) = \frac{g}{2\omega} k_\infty = \frac{\omega^2}{g}$$

for which (7) can be solved for the finite depth wavenumber k . Out in the deep water a gravity wave with frequency ω has an associated wave number k_∞ and group velocity $c_g(\infty)$ given by (10). The amplitude of this harmonic wave is $\tilde{h}_\infty(k_\infty)$ and is determined by the deep-water power spectrum. As this wave propagates into shallower water (of depth d) its wave number changes to k , satisfying (7) and its group velocity is modified appropriately; the amplitude of the associated harmonic component is $\tilde{h}_d(k)$. The energy flux carried by the wave is constant; thus we can equate the product of the square modulus of the amplitude and group velocity pertaining to depth d with its deep-water value. In this way we find that

Equation 11

$$|\tilde{h}_d(k)|^2 = \frac{|\tilde{h}_\infty(k_\infty)|^2}{\tanh(kd) + kd \operatorname{sech}^2(kd)}$$

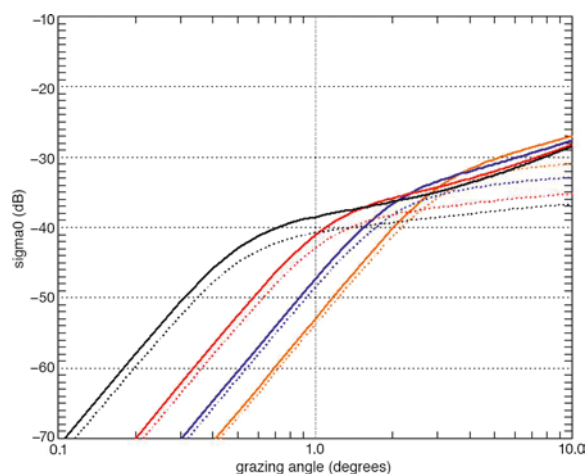
This in effect allows us to relate the deep water and finite depth power spectra. Finally account must be taken of the elliptical character of the fluid motions characteristic of finite depth – loosely speaking, this provides us with a physical manifestation of Tassendorf's variable parameter μ that now enhances wave breaking in the shallows.

These modifications can now be incorporated into the expectation values characterising the statistical behaviour of the elements of the Jacobian matrix introduced above, and the associated breaking area can be evaluated through (6). Preliminary results show a sensible increase in breaking area of water with a depth less than wavelengths with significant weight in the power spectrum. Thus we obtain enhanced wave breaking in addition to the wave spectrum changes described above.

Clutter RCS in the littoral

In order to apply the modelling above to evaluate expected sea clutter NRCS in littoral environments it is necessary to set up a model of the detailed topography and weather conditions. This is currently underway and will be reported later. The results will be very dependent upon the conditions and area evaluated. Thus users of radar systems will need to run this type of model in their own environment in order to evaluate equipment, plan missions and optimise radar usage.

5



Normalised radar cross section versus grazing angle calculated for a wind speed of 7.6 m/s and fetches of 100 km, 8 km, 2 km and 700 m, with vertical (solid lines) and horizontal (dotted lines) polarisations.

An indication of the effect of littoral water on sea clutter may be obtained by considering the limited fetch example discussed above. Figure 5 shows the change of NRCS at X-band for a wind speed of 7.6 m/s as a function of fetch. One might expect that the clutter would be less for short fetches due to the reduced wave height. Figure 5 shows that this is the case below about 1 degree grazing angle. Above that angle, however, the increased breaking for short fetch, due to the choppy nature of the sea, causes the trend to reverse and shorter fetches result in higher NRCS. This is particularly apparent for horizontal polarisation, where the spikes from breaking waves dominate the return.

Conclusions

The work described above extends physical modelling of low grazing angle sea clutter from open seas to littoral environments.

Thus far we have only considered average clutter power (NRCS). For many types of radar other aspects of the clutter (e.g., Doppler spectrum, amplitude statistics, correlation, etc) are equally important for characterising performance [10]. These are currently being addressed using the same underlying ocean modelling that we have used here for NRCS.

Acknowledgements

The work reported in this paper was funded by the Electro-Magnetic Remote Sensing (EMRS) Defence Technology Centre, established by the UK Ministry of Defence and run by a consortium of SELEX Galileo, Thales UK, Roke Manor Research and Filtronic.

References

1. T. Elfouhaily, B. Chapron and K. Katsaros, 'A unified directional spectrum for long and short wind-driven waves', *J. Geophys. Res.*, **102(C7)**, 15781–15796, (1997).
2. R.J.A. Tough, K.D. Ward, PW Shepherd, 'Electromagnetic Modelling of Radar Sea spikes', 1st EMRS–DTC Technical Conference, Edinburgh, Paper A2, (2004).
3. J. Lighthill, 'Waves in Fluids'. Chap. 3 University Press, Cambridge, 1978.
4. F.J. von Gerstner, 'Theorie der wellen', *Abhandlungen der Koniglichen Bohmischen Gesellschaft der Wissenschaft*, **1**, pp. 1–65, (1804).
5. D.B. Creamer, F. Henyey, R. Schult, and J. Wright, 'Improved Linear Representation of Ocean Surface Waves', *J. Fluid Mech.*, **205**, pp. 135–161, (1989).
6. J. Tessendorf, 'Simulating ocean water. In *Simulating Nature: From Theory to Applications*', D. S. Ebert, Ed., no. 26 in SIGGRAPH 99 Course Notes. (1999).
7. M.S. Longuet Higgins, 'On the overturning of gravity waves', *Proc. Roy. Soc.*, **A376**, 377–400, 1981.
8. R.J.A. Tough and K.D. Ward, 'First progress report on Littoral Sea clutter modelling', TWR/R094/01, 2007.
9. M. Katzin, 'On the mechanisms of radar sea clutter', *Proc. IRE*, **45**, 44–54, (1957).
10. K.D. Ward, R.J.A. Tough and S. Watts, 'Sea Clutter: Scattering, the K Distribution and Radar Performance', Institution of Engineering and Technology, 2006.
11. M.N. Gamito and F.K. Musgrave, 'An accurate model for wave refraction over shallow water', *Computer Graphics*, **26(2)**, pp. 299–307 (2002).
12. T. Lamont-Smith, A.M. Jackson, P.W. Shepherd and R.D. Hill, 'Low grazing angle radar imaging experiments over the South Falls sandbank', *Int. J. Remote Sensing*, **26**, No. 5, pp 937–966, 10 March 2005.